Design of a tomographic projection lithography system and material for roll-to-roll fabrication of 3D microstructures

Joseph Toombs, Chi Chung Li, Hayden Taylor

Department of Mechanical Engineering, University of California, Berkeley, Berkeley, CA, USA

ABSTRACT

Large area arrays of three-dimensional microstructures are widely used in electronics, surface engineering, microfluidic chemical synthesis and diagnostics, and filtration. Current roll-to-roll (R2R) fabrication techniques have improved production speed of arrays of primarily two-dimensional structures, but they must resort to sequential multi-step lamination or deposition processes if more complex 3D structures are desired. We describe a single-step volumetric light-based approach that is enabled by tomographic light exposure, called R2R computed axial lithography (CAL). We describe the geometric freedom of the system and analyze the resolution of the dynamic projection optical system that supports lateral scanning and axial focus scanning. Additionally, we introduce a solid-phase photoresist that is compatible with tomographic light exposure of material coated on a web and capable of feature sizes as small as 20 µm. These developments illustrate how the R2R CAL process could streamline R2R fabrication of unprecedented 3D microstructures with reentrant features and internal voids.

Keywords: imprint lithography, computed axial lithography, tomography

1. INTRODUCTION

Roll-to-roll fabrication (R2R) has emerged as a revolutionary technique to expedite production of micro and nanostructures in the semiconductor lithography industry. R2R imprint lithography (R2RIL) is the most common process within the class of R2R technologies. A micromachined master imprint roller prescribes the geometry while heat or UV light is used to emboss thermoplastic or polymerize photoresist coated on a web substrate. Because the imprint roller must be demolded from the microstructures, single-step R2RIL is typically limited to production of simple microstructures including hydro/oleophobic surfaces[1], wire grid polarizers[2], antireflective surfaces[3], and primarily 2D microfluidic devices[4].

When combined with sequential lamination or deposition, multi-step imprint processes can produce more complex geometries including multilayer electrode assemblies[5]. A recent alternative additive manufacturing technique solidifies photoresist onto a web as it is drawn out of a vat (RAMP)[6]. However, the sequential deposition or solidification of material is not optimal for freeform high-aspect ratio microstructures with reentrant features and internal voids which have applications in mechanical metamaterials[7], microfluidics for chemical synthesis and diagnostics[8–10], low fouling filtration and desalination[11], and biocompatible scaffolding for 3D tissue engineering[12]. In RAMP, when the web is drawn from the vat, reflowing of the liquid free surface imposes speed limitations and certain geometries may require sacrificial support structures. In deposition techniques, the interlayer registration constraints to produce such geometries imply that the machinery must perform material deposition or solidification and subsequent development of delicate structures with a high degree of precision layer-to-layer over the entire substrate.

An alternative to sequential laminar construction is volumetric processing such as laser interference lithography (LIL) and computed axial lithography (CAL). LIL is a light-based interferometric technique which produces a 3D light field at the intersection of multiple coherent laser beams. While LIL can fabricate large arrays of microstructures it is limited to production of periodic structures[13], CAL has geometric flexibility to produce arbitrary aperiodic structures[14]. Briefly, in CAL, a 3D light dose pattern is accumulated in a cylindrical container of negative-acting photopolymer from azimuthally multiplexed light projections. The light projections are precomputed using tomographic principles from computed tomography and intensity modulated radiation therapy. Once the volumetrically described light dose surpasses the photopolymer's gelation threshold, the target structure forms simultaneously.

Here we propose the optical design of a R2R CAL system to streamline production of arbitrary arrays of 3D microstructures and provide analysis of the system in terms of optical resolution and geometric flexibility performance metrics. We also introduce a specialized solid-phase free-radical-mediated photopolymer which enables CAL fabrication on a web.

2. RESULTS/DISCUSSION

The R2R CAL system we propose utilizes similar tomographic light superposition principles to conventional CAL. However, there are additional constraints which the photopolymer substrate (cylindrical container vs. web) imposes on the system, namely, computational, optical, and material constraints.

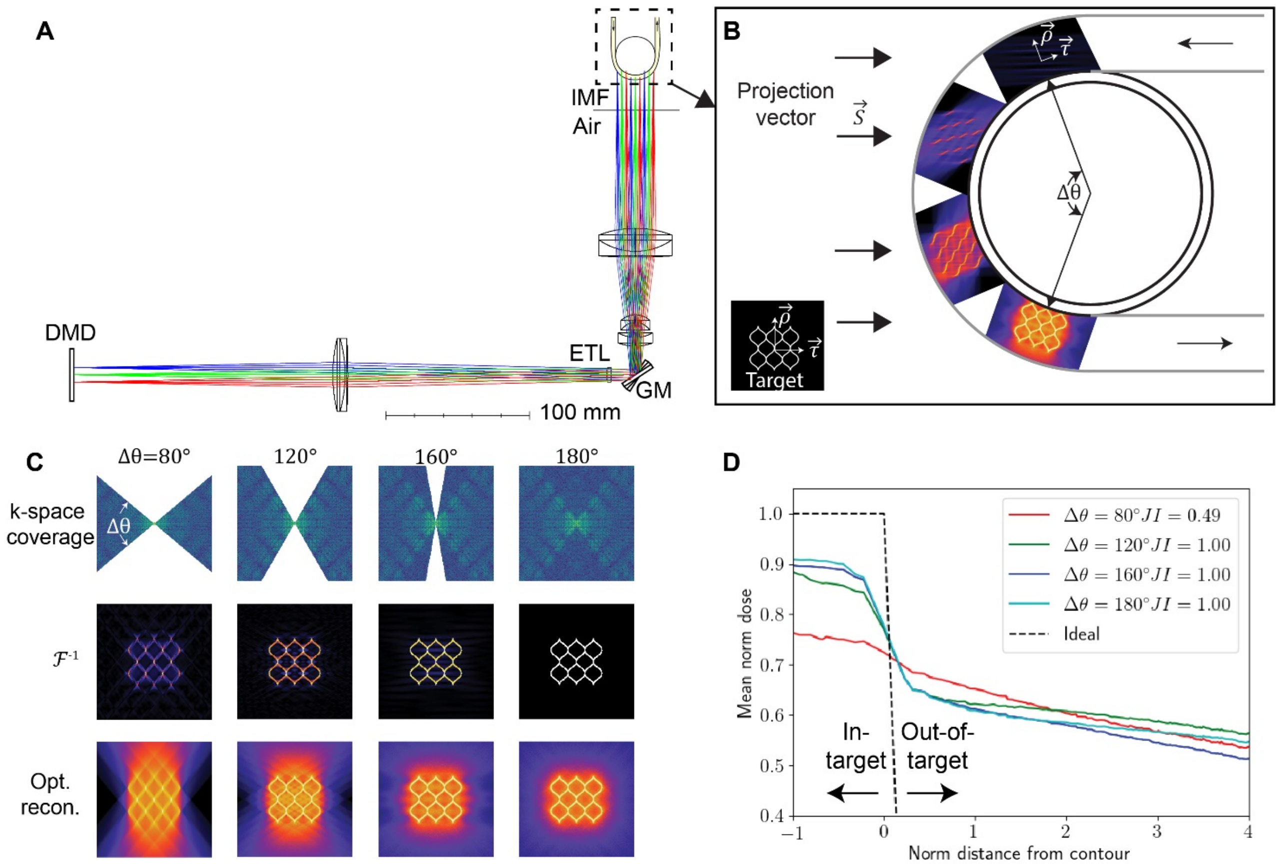

Figure 1. (A) Optical diagram of R2R CAL system. (B) Dose accumulates as the web traverses the backing roller and the τ-ρ coordinate system of an exposed region of the web rotates through $\Delta\theta$ relative to the projection vector $\vec{S}$. (C) Geometric flexibility: Top row: Fourier transform of the target pattern (inset of B). Regions that are inaccessible (due to $\Delta\theta < \pi$) are omitted. Middle row: inverse Fourier transform of the top row which is the ideal reconstruction if projection magnitude is unconstrained (i.e., if negative intensities are allowed). Bottom row: optimal reconstruction resulting from positivity constrained projections. (D) Mean normalized dose as a function of the normalized distance from the contour of the target geometry for angles shown in C. Adapted from Toombs *et al.*[16]

First, we assume the projected patterns have low divergence in the photoresist, i.e., long depth of focus, and we computationally model the digital light projections as 2D projections through a 3D grid which accumulates the light dose contribution from each angle θ. In CAL, normally we would have $\theta \in [0, \pi)$, however, in the R2R CAL configuration the range of angles $\Delta\theta = \theta_{max} - \theta_{min}$ is not guaranteed to be equal to π because of physical constraints discussed later, i.e., $\Delta\theta \leq \pi$. For $\Delta\theta < \pi$, the Fourier slice theorem[15] implies that some spatial frequency information is irrecoverable and, consequently, some geometric flexibility in structures producible by R2R CAL is lost. Increasing the DMD sampling rate by further demagnification or obtaining a DMD with higher native pixel density would increase the attainable maximum spatial frequency along each angular slice within k-space, but it would not enable recovery of spatial frequency content outside $\Delta\theta$. In Figure 1B, the Fourier transform or k-space representation of the 2D target geometry in Figure 1A is shown with hypothetical regions that are inaccessible omitted. The optimal reconstruction resembles the target closer with increasing $\Delta\theta$ and correspondingly increased out-of-plane resolution as expected. In Figure 1D, we quantify the optimality of the reconstruction with the Jaccard similarity index[14] (JI) and dose contrast between the target and the non-target regions. For this particular structure, 100% JI was achieved for $\Delta\theta = 120°$ and increasing $\Delta\theta$ only marginally improved the dose contrast (i.e., the maximum absolute value of the gradient between in-target and out-of-target regions). This suggests that geometries which have a significant fraction of their spatial frequency content concentrated within $\Delta\theta$ may be faithfully reconstructed.

The web substrate requires that we depart from the optical design of conventional CAL in which the focal plane is located on the axis of rotation of the cylindrical container. From the previous discussion of computation of the projection light patterns, it is evident that increasing $\Delta\theta$ increases geometric flexibility, so the optical system is designed to maximize $\Delta\theta$. On a flat substrate, accommodating large incident angles, i.e. angles near $\pm\pi/2$ relative to the surface normal $\vec{\rho}$, is challenging because the optical path length is inversely proportional to the cosine of the incident angle, assuming no refraction at the surface. By taking advantage of the cylindrical geometry of a conveying roller, the optical path length was minimized for large incident angles (Fig. 1B). In an open-air system in which patterned light is propagating through air and is incident on the curved photoresist interface, Fresnel reflection losses should be compensated in the exposure dose reconstruction simulation. Although, addition of a refractive index matching fluid (IMF) (Figure 1A) provides a flat air-fluid interface and eliminates the curved air-photoresist interface when the fluid's refractive index is matched to the photoresist refractive index. While this could introduce implementation challenges, it allowed us to achieve a large theoretical $\Delta\theta$ and to neglect Fresnel reflection in the exposure dose simulation.

Optically, it is not possible to achieve the zero divergence '2D light projection' that was assumed to simplify computation. Consequently, in a static optical system, there will always be a plane of best focus. Though, by designing a low étendue system, i.e., a system with small product of source size and source solid angle, we can minimize divergence at the cost of higher requirements on the laser source quality. Our proposed system was designed to minimize divergence yet tolerate the remaining nonzero divergence by including dynamic components. The focal plane can be scanned axially and diametrically with an electrically tunable lens (ETL) and galvanometer mirror scanner (GM) to maintain high resolution over the entire face the cylindrical backing roller (Fig. 1A). We achieved high modulation transfer function (MTF) (MTF $\geq$ 0.4) — the level of contrast transfer of spatial frequencies of the object to image space through an optical system — for spatial frequencies up to 60 cycles/mm.

In the R2R configuration, there is increased demand on the refresh rate of the spatial light pattern because features are written at a distance from the rotation axis and consequently the web has higher tangential velocity than material near the rotation axis. We modeled the motion of the web during exposure with a convolutional model using a blurring kernel dependent on web speed and feature orientation relative to $\vec{\rho}$. The results of the model suggests that it is important to consider the target geometry and $\Delta\theta$ of the system in coordination with the speed requirements to achieve high fidelity and high contrast light exposure. We refer the reader to Toombs *et al.* [16] for more in depth analysis of this topic.

In order to perform light exposure on a web in an arbitrary orientation relative to gravity, the photopolymer should be a liquid with sufficient viscosity to avoid motion during exposure or better, a solid which does not move relative to the web. Typical photolithography resists consisting of high solid polymer content and a solvent are dispensed in liquid form. After evaporation of the solvent, the material is a solid. While the approach works well for films of sub-micron to hundreds of microns thickness, for films above 1 mm thickness this approach becomes impractical due to increasingly long solvent diffusion and evaporation times[17]. For many applications, films about 1–2 mm in thickness would better suit the intended end products, e.g., biofabrication scaffolding and filter dividers.

To create a solid-phase photopolymer capable of forming 1–2 mm freestanding films, we formulated an organogel photopolymer. Organogels typically consist of an organic liquid or liquids and a gelling agent which is soluble in organic solvents[18]. In particular, we formed an organogel with 5% (wt/wt) ethyl cellulose (EC) in trimethylolpropane triacrylate (TMPTA) by mixing both components at 110°C for 50 minutes. To this mixture was added 0.01 M concentration of 2-Benzyl-2-dimethylamino-1-(4-morpholinophenyl)-butanone-1 (Irgacure 369) photoinitiator. After mixing, at elevated temperature the liquid could be dispensed onto a

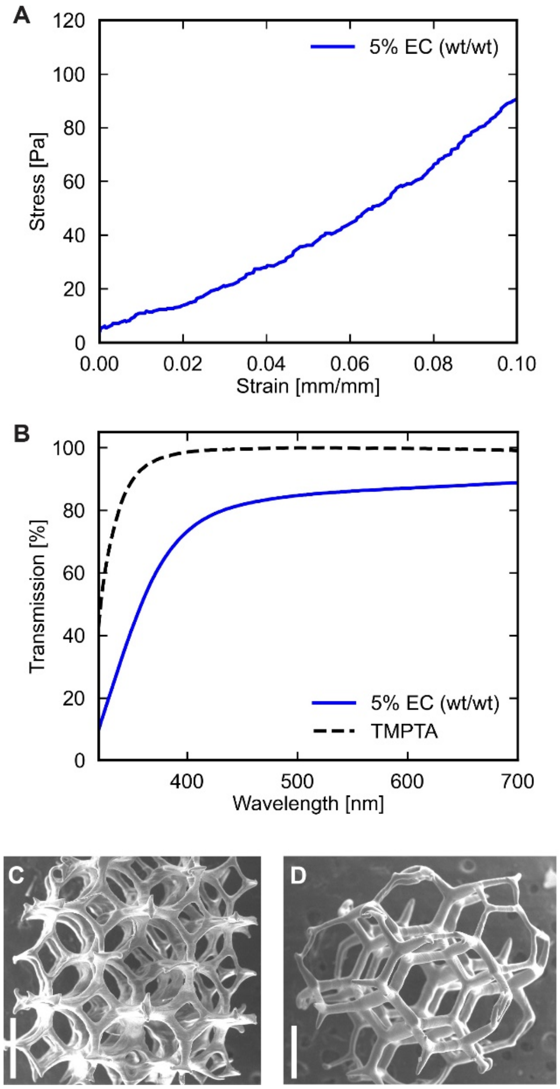

Figure 2. (A) Stress-strain data from compression of casted 16 mm diameter EC gel cylinder. (B) UV-VIS transmission of EC gel without photoinitiator and TMPTA alone. (C, D) Scanning electron micrographs of lattices printed in EC gel photoresist. Scale bars: 500 µm.

substrate or cast into molds for material characterization. As the mixture cools, physical thermoreversible crosslinks form between EC monomer and immobilize the TMPTA in a semi-solid network. At room temperature the organogel had a Young's modulus of about 1 kPa (Figure 2A) and became a liquid with viscosity of 100 cP at elevated temperatures (65°C).

Since the refractive index of the EC gel network (1.47[19]) is close to that of TMPTA (1.4735[20]), in the solid phase, the organogel has high transmission over the visible range and moderate transmission in the UV range. Figure 2B shows the UV-VIS collimated transmission over a 1 cm pathlength without photoinitiator with 75% transmission at 405 nm (h-line) and 55% transmission at 365 nm (i-line).

To validate the EC gel as a high contrast photopolymer, we demonstrated printing of lattice structures with minimum feature size as small as 20 µm (Figure 2 C–D). The material exhibits sufficient contrast and oxygen inhibition period to achieve microscale tomographic patterning. To develop the structures, we heated the EC gel to 100°C and immersed it in isopropyl alcohol for 30 minutes. Then, the structures were removed and allowed to dry in air. Although these structures were fabricated on a conventional CAL apparatus[21], the results demonstrate that this material is well suited for use in the proposed R2R CAL apparatus.

3. CONCLUSION

We described a volumetric approach to R2R production of microstructures based on the tomographic light-based technique computed axial lithography. Our proposed process eliminates sequential deposition and lamination steps that are required by imprint-based R2R techniques. We analyzed the geometric freedom of the R2R CAL technique and constructed an optical model of the system which suggests approximately 16 µm line-space optical resolution. Additionally, we modeled the motion blur due to relative web-light-pattern motion and found that it is critical to consider target geometry and orientation on the web in coordination with speed requirements to reach the maximum resolution of which the optical system is capable. Finally, we described a gel photoresist compatible with tomographic exposure that enables 1–2 mm thick coatings on a web to pass over the cylindrical backing roller in any orientation with respect to gravity.

ACKNOWLEDGMENTS

The authors thank Sui Man Luk for engaging conversations about gel materials. This work was supported primarily by the National Science Foundation under Cooperative Agreement No. EEC-1160494. Any opinions, findings and conclusions or recommendations expressed in this material are those of the author(s) and do not necessarily reflect the views of the National Science Foundation.

REFERENCES

[1] Kodihalli Shivaprakash, N., Zhang, J., Nahum, T., Barry, C., Truong, Q. and Mead, J., "Roll-to-Roll Hot Embossing of High Aspect Ratio Micro Pillars for Superhydrophobic Applications," Int. Polym. Process. **34**(5), 502–512 (2019).

[2] Ahn, S. H. and Guo, L. J., "Large-area roll-to-roll and roll-to-plate Nanoimprint Lithography: A step toward high-throughput application of continuous nanoimprinting," ACS Nano **3**(8), 2304–2310 (2009).

[3] Jacobo-Martín, A., Rueda, M., Hernández, J. J., Navarro-Baena, I., Monclús, M. A., Molina-Aldareguia, J. M. and Rodríguez, I., "Bioinspired antireflective flexible films with optimized mechanical resistance fabricated by roll to roll thermal nanoimprint," Sci. Rep. **11**(1), 2419 (2021).

[4] Liedert, C., Rannaste, L., Kokkonen, A., Huttunen, O.-H., Liedert, R., Hiltunen, J. and Hakalahti, L., "Roll-to-Roll Manufacturing of Integrated Immunodetection Sensors," ACS Sensors **5**(7), 2010–2017 (2020).

[5] Chen, J., Liu, H., Huang, Y. and Yin, Z., "High-rate roll-to-roll stack and lamination of multilayer structured membrane electrode assembly," J. Manuf. Process. **23**, 175–182 (2016).

[6] Ou, J. and Neumann, F., "METHODS AND APPARATUS FOR FABRICATION WITH A MOVABLE SHEET," 11,104,060 B2 (2021).

[7] Zheng, X., Smith, W., Jackson, J., Moran, B., Cui, H., Chen, D., Ye, J., Fang, N., Rodriguez, N., Weisgraber, T. and Spadaccini, C. M., "Multiscale metallic metamaterials," Nat. Mater. **15**(10), 1100–1106 (2016).

[8] Gale, B., Jafek, A., Lambert, C., Goenner, B., Moghimifam, H., Nze, U. and Kamarapu, S., "A Review of Current Methods in Microfluidic Device Fabrication and Future Commercialization Prospects," Inventions **3**(3), 60 (2018).

[9] Cui, P. and Wang, S., "Application of microfluidic chip technology in pharmaceutical analysis: A review," J. Pharm. Anal. **9**(4), 238–247 (2019).

[10] Kotz, F., Risch, P., Helmer, D. and Rapp, B. E., "High-Performance Materials for 3D Printing in Chemical Synthesis Applications," Adv. Mater. **31**(26) (2019).

[11] Sreedhar, N., Thomas, N., Al-Ketan, O., Rowshan, R., Hernandez, H., Abu Al-Rub, R. K. and Arafat, H. A., "3D printed feed spacers based on triply periodic minimal surfaces for flux enhancement and biofouling mitigation in RO and UF," Desalination **425**(September), 12–21 (2018).

[12] Kundu, J., Pati, F., Hun Jeong, Y. and Cho, D.-W., "Biomaterials for Biofabrication of 3D Tissue Scaffolds," [Biofabrication], Elsevier, 23–46 (2013).

[13] Lin, Y., Harb, A., Lozano, K., Xu, D. and Chen, K. P., "Five beam holographic lithography for simultaneous fabrication of three dimensional photonic crystal templates and line defects using phase tunable diffractive optical element," Opt. Express **17**(19), 16625 (2009).

[14] Kelly, B. E., Bhattacharya, I., Heidari, H., Shusteff,

M., Spadaccini, C. M. and Taylor, H. K., “Volumetric additive manufacturing via tomographic reconstruction,” Science (80-.). **363**(6431), 1075–1079 (2019).

[15] Kak, A. C., Slaney, M. and Wang, G., “Principles of Computerized Tomographic Imaging,” Med. Phys. **29**(1), 107–107 (2002).

[16] Toombs, J. and Taylor, H. K., “Design of a tomographic projection lithography process for roll-to-roll fabrication of 3D microstructures,” Nov. Patterning Technol. 2021(February), E. M. Panning and J. A. Liddle, Eds., 11, SPIE (2021). (invited)

[17] Moreau, W. M., “Semiconductor Lithography: Principles, Practices, and Materials,” [Semiconductor Lithography: Principles, Practices, and Materials] (1988).

[18] Guenet, J.-M., [Organogels: Thermodynamics, Structure, Solvent Role, and Properties] (2016).

[19] McKeen, L. W., [Film Properties of Plastics and Elastomers], Elsevier (2012).

[20] “Alfa Aesar™ Trimethylolpropane triacrylate, stabilized.”, 2021, <https://www.fishersci.com/shop/products/trimethylolpropane-triacrylate-stabilized-3/AA1644522>.

[21] Taylor, H. K., Toombs, J., Luk, S. M., Feili, S., Heidari, H., Li, C. C., Bansal, V., Coulson, K. and Goli, E., “Modeling of light propagation in computed axial lithography with photopolymers,” Emerg. Digit. Micromirror Device Based Syst. Appl. XIII, B. L. Lee and J. Ehmke, Eds., 4, SPIE (2021). (invited)